



## On the wavelet Galerkin method for solving the fractional Fredholm integro-differential equations

Sharareh Ranjbari<sup>1</sup>, Mahdi Baghmisheh<sup>1,\*</sup>, Mohammad Jahangiri Rad<sup>1</sup>, and Behzad Nemati Saray<sup>2</sup>

<sup>1</sup>Department of Mathematics, Ta.C., Islamic Azad University, Tabriz, Iran.

<sup>2</sup>Department of Mathematics, Institute for Advanced Studies in Basic Sciences (IASBS), Zanjan 45137-66731, Iran.

### Abstract

An effective scheme is presented to estimate the numerical solution of fractional integro-differential equations (FIDEs). In the present method, to obtain the solution of the FIDEs, they must first be reduced to the corresponding Volterra-Fredholm integral equations (VFIEs) with a weakly singular kernel. Then, by applying the matrix that represents the fractional integral (FI) based on biorthogonal Hermite cubic spline scaling bases (BHC-SSb), and using the wavelet Galerkin method, the reduced problem can be solved. The combination of singularity and the challenge related to nonlinearity poses a formidable obstacle in solving the desired equations, but our method overcomes them well. An investigation of the method's convergence is provided, and it verifies that the convergence rate is  $O(2^{-J})$  where  $J \in \mathbb{N}_0$  is the refinement level. The verification of convergence has also been demonstrated through the presentation of several numerical examples. Compared to other methods, the results obtained show better accuracy.

**Keywords.** Wavelet Galerkin method, Fractional integro-differential equation, Biorthogonal wavelet, Hermite cubic splines, Convergence analysis.

**2010 Mathematics Subject Classification.** 65N60, 47G20, 65T60, 65D07, 65Bxx.

### 1. INTRODUCTION

Integro-differential equations are frequently used in scientific applications, particularly when transforming initial or boundary value problems into integral equations. These equations also appear in modeling some phenomena, including circuit analysis, epidemiology, and other fields. They contain both integral and differential operators, with the derivative potentially of any order. It is worth noting that to obtain the specific solution of these equations, the initial conditions must be given. The general  $\eta$ -order integro-differential equation is given by

$$w^{(\eta)}(x) + \int_{\Omega} g(t, w(t))dt = f(x, w(x)), \quad w^{(\nu)}(0) = w_{\nu}, \quad \nu = 0, \dots, \eta - 1,$$

where  $f$  and  $g$  are analytical functions that can be either linear or nonlinear.

As we know, it is generally difficult, and sometimes impossible, to obtain the exact solution of integro-differential equations. Meanwhile, the main goal of applied mathematics is to develop numerical algorithms that achieve better accuracy or provide efficient solutions.

**1.1. A glance over the FIDEs.** This paper aims to implement and develop the Galerkin method for finding numerical solutions of the fractional integro-differential equations (FIDEs)

$${}^C \mathcal{D}_0^{\kappa} w(x) = c_1 f(x, w(x)) + c_2 \int_{\Omega} k(x, t)g(w(t))dt, \quad x \in \Omega, \quad (1.1)$$

with initial conditions

$$w^{(\nu)}(0) = w_{\nu}, \quad \nu = 0, \dots, \eta - 1, \quad (1.2)$$

Received: 20 June 2024 ; Accepted: 06 October 2024.

\* Corresponding author. Email: baghmishe@iaut.ac.ir.

where  $\Omega = [0, 1]$ ,  $c_1$  and  $c_2$  are constants, and  ${}^C\mathcal{D}_0^\kappa$  denotes the Caputo fractional derivative (CFD) of order  $\kappa$  ( $\kappa \in \mathbb{R}^+$ ). Here,  $\eta = \kappa$  if  $\kappa \in \mathbb{N}$ , and  $[\kappa] + 1 := \eta \in \mathbb{N}$ , if  $\kappa \notin \mathbb{N}$ .

In (1.1),  $f : \Omega \times \mathbb{R} \rightarrow \mathbb{R}$  is a sufficiently smooth function, which may be linear or nonlinear,  $k := \Omega \times \Omega \rightarrow \mathbb{R}$  is a continuous, and the linear or nonlinear function  $g : C(\Omega) \rightarrow \mathbb{R}$  satisfies the Lipschitz condition

$$|g(w_1) - g(w_2)| \leq \rho |w_1 - w_2|, \quad (1.3)$$

with Lipschitz constant  $\rho > 0$ .

Fractional integro-differential equations (FIDEs) (1.1) arise in modeling various physical phenomena, such as the epidemic process [3], viscoelasticity [14], and glass-forming process [2]. Numerical methods for solving such equations have been explored in several works, a few of which we highlight here. In [25], the authors employed the Adomian decomposition method to solve FFIDEs. Later, Momani et al. [26] extended this approach to systems of FFIDEs. Rawashdeh [30] applied a spline-based collocation method to solve the problem, while [4] utilized the fractional differential transform scheme for solving FIDEs.

Zhu et al. [39] have employed the Galerkin method, based on Chebyshev wavelets, to study the specific case of Equation (1.1), namely,

$${}^C\mathcal{D}_0^\kappa w(x) - \int_{\Omega} k(x, t)[w(t)]^v dt = f(x), \quad v > 1. \quad (1.4)$$

In [39], the action of the fractional integral (FI) operator on the Chebyshev wavelet is represented by an operational matrix, and Equation (1.4) is solved using the Galerkin method combined with an integration operational matrix.

Saeedi et al. [33] derived the operational matrix of FI for CAS wavelets and applied it to solve Equation (1.4) using the wavelet Galerkin method.

**1.2. A glance at fractional differential equations.** In recent years, fractional differential equations (FDEs) and their applications in modeling physical phenomena have garnered significant attention from researchers. The literature reveals traces of these equations in diverse phenomena, including solid mechanics [31], anomalous transport [23], viscoelastic materials [7], fluid-dynamic traffic [16], economics [8], colored noise [20], continuum and statistical mechanics [19], and nonlinear oscillation of earthquakes [15], among others. While several propose techniques for analytical solutions, these methods often fail for complex equations, necessitating numerical approaches. Among effective numerical methods are the Adams scheme [13, 22, 35], Adomian decomposition [24], Bernoulli wavelet [29], finite difference [21], polynomial interpolation [6], predictor-corrector [10], B-spline wavelet collocation [18], piecewise quadratic polynomial interpolation [38], Alpert's multiwavelet [5], and Legendre wavelet [34].

**1.3. A glance at multiwavelets.** Wavelets have gained prominence in mathematical applications, particularly for solving differential equations. Multiwavelets, in particular, offer advantages over scalar wavelets due to their orthogonality, symmetry, high vanishing moments, and closed-form expressions. Unlike biorthogonal wavelets, multiwavelets achieve higher vanishing moments without increasing the support of their basis functions. They are constructed via translation and dilation of multiple generators satisfying a vector refinement relation. Notable examples include Alpert's multiwavelets [1, 36, 37] and biorthogonal Hermite cubic spline (BHCS) wavelets [11], which are widely used in numerical analysis. Section 2 will detail the construction and properties of BHCSb (biorthogonal Hermite cubic spline scaling bases).

The wavelet system offers a range of useful properties that can be employed in various applications. Wavelets can be used to construct operational matrices that are useful for representing different operators, such as derivatives, integrals, etc. One of the key benefits of using operational matrices obtained by wavelets is that they enable sparsity, meaning that for this type of function, the number of operational matrix elements is much smaller compared to others. As you know, this can help reduce processing costs and make operations more efficient. Another important feature of this type of basis is that they have multi-scale properties, and this property is achieved with the help of the parameter  $J$ . That is, with the increase of  $J$ , the bases are refined and the approximation accuracy increases. This property can be very useful, especially when the function has a discontinuity or does not have a continuous derivative. In such cases, we choose the parameter  $J$  to be large. For large  $J$ , the error gets bounded by the fact that the interval is small.



**1.4. The main framework and goal of this paper.** In the current study, we aim to implement and develop the Galerkin method to find the numerical solution of the FIDEs. The framework of this paper is as follows:

- After introducing some preliminary definitions and concepts of fractional calculus, we introduce BHCSSb in section 2.
- Section 3 relates to implementing the Galerkin method based on BHCSSb to solve Eq. (1.1). A convergence investigation is also conducted in this section.
- In section 4, some numerical experiments are provided to show how accurate and useful the method is.
- Finally, we complete this work with a conclusion in section 5.

## 2. PRELIMINARIES

Note that due to the importance of the topic, it is worth re-reading the preliminary concepts of fractional calculus. For this reason, we start this subsection with these concepts, and then provide a review of BHCSSb along with their characteristics.

### 2.1. Required fractional concepts.

**Definition 2.1.** Given  $\kappa \in \mathbb{R}^+$ , the FI operator  $\mathcal{I}_a^\kappa$  of order  $\kappa$  is specified by

$$\mathcal{I}_0^\kappa(v)(x) := \frac{1}{\Gamma(\kappa)} \int_0^x (x-z)^{\kappa-1} v(z) dz, \quad x \in [0, 1], \tag{2.1}$$

where  $\Gamma(\kappa)$  denoted the Gamma function.

Given the power function, its fractional integration is also a power function. That is

$$\mathcal{I}_0^\kappa(x^\alpha) = \frac{\Gamma(\alpha+1)}{\Gamma(\kappa+\alpha+1)} x^{\kappa+\alpha}. \tag{2.2}$$

It can be verified that  $\mathcal{I}_0^\kappa$  is bounded. We present the following lemma to determine this bound (cf. Lemma 2.1 (a), [17]).

**Lemma 2.2.** *There is an estimation of the bound of the fractional integral operator  $\mathcal{I}_0^\kappa$  in  $L_q([0, 1])$ , viz.,*

$$\|\mathcal{I}_0^\kappa(w)\|_q \leq \frac{1}{\Gamma(\kappa+1)} \|w\|_q, \quad 1 \leq q \leq \infty. \tag{2.3}$$

**Definition 2.3.** For  $\kappa \in \mathbb{R}^+$  and  $[\kappa] + 1 := \eta \in \mathbb{N}$ , let  $\mathcal{D}^\eta := \frac{d^\eta}{dx^\eta}$ . Then  ${}^R\mathcal{D}_0^\kappa$  denotes the Riemann-Liouville fractional derivative (RLFD) operator

$${}^R\mathcal{D}_0^\kappa(w)(x) := \mathcal{D}^\eta \mathcal{I}_0^{\eta-\kappa}(w)(x) = \frac{1}{\Gamma(\eta-\kappa)} \mathcal{D}^\eta \int_0^x (x-z)^{\eta-\kappa-1} w(z) dz.$$

**Definition 2.4.** [17] For  $\kappa \in \mathbb{R}^+$  and  $[\kappa] + 1 := \eta \in \mathbb{N}$ , the Caputo fractional derivative (CFD)  ${}^C\mathcal{D}_0^\kappa$  is defined as

$${}^C\mathcal{D}_0^\kappa(w)(x) := \frac{1}{\Gamma(\eta-\kappa)} \int_0^x \frac{w^{(\eta)}(z) dz}{(x-z)^{\kappa-\eta+1}} =: \mathcal{I}_0^{\eta-\kappa} \mathcal{D}^\eta(w)(x). \tag{2.4}$$

**Lemma 2.5.** (cf. Corollary 2.3 (a), [17]). *There is an estimation of the bound of the norm of the CFD operator  ${}^C\mathcal{D}_0^\kappa$ , viz.,*

$$\|{}^C\mathcal{D}_0^\kappa(w)\|_C \leq \frac{1}{\Gamma(\eta-\kappa)(\eta-\kappa+1)} \|w\|_{C^\eta}, \tag{2.5}$$

where  $\kappa \in \mathbb{R}^+$ ,  $\kappa \notin \mathbb{N}_0$  and  $\eta = -[-\kappa]$ .



**2.2. Biorthogonal Hermite cubic spline scaling bases.** A brief introduction to BHCSSb is provided in this subsection. Following [11], BHCSSb consists of two piecewise functions

$$\phi^1(x) = \begin{cases} -2x^3 - 3x^2 + 1, & -1 \leq x \leq 0, \\ 2x^3 - 3x^2 + 1, & 0 \leq x \leq 1, \\ 0, & \text{o.w.} \end{cases} \tag{2.6}$$

and

$$\phi^2(x) = \begin{cases} x + 2x^2 + x^3, & -1 \leq x \leq 0, \\ x - 2x^2 + x^3, & 0 \leq x \leq 1, \\ 0, & \text{o.w.} \end{cases} \tag{2.7}$$

Note that  $\phi^1, \phi^2 \in C^1(\mathbb{R})$  and satisfy the Hermite interpolation conditions [11]:

$$\phi^1(\theta) = \delta_{0,\theta}, \quad \phi^2(\theta) = 0, \quad (\phi^1)'(\theta) = 0, \quad (\phi^2)'(\theta) = \delta_{0,\theta}, \quad \forall \theta \in \mathbb{Z}, \tag{2.8}$$

where  $\delta_{i,j}$  denotes the Kronecker delta.

To satisfy multiresolution analysis (MRA) properties, we consider a subspace of  $L_2([0, 1])$ :

$$V_J := span\{\{\phi_{J,b}^k | b \in \mathcal{J}, k = 1, 2\} \cup \{\sqrt{2}\phi_{J,0}^1|_{[0,1]}, \sqrt{2}\phi_{J,2^J}^1|_{[0,1]}\}\}, \tag{2.9}$$

where  $J \in \mathbb{N}_0, \mathcal{J} := \{1, \dots, 2^J - 1\}$ , and  $\phi_{J,b}^k := \phi^k(2^J \cdot - b)$ .

From MRA, the vector function  $\phi = (\phi^1, \phi^2)$  satisfies the refinement relation:

$$\phi(x) = \sum_{b \in \mathbb{Z}} H_b \phi(2x - b), \tag{2.10}$$

with coefficient matrices:

$$H_{-1} = \begin{pmatrix} 1/2 & 3/4 \\ -1/8 & -1/8 \end{pmatrix}, \quad H_0 = \begin{pmatrix} 1 & 0 \\ 0 & 1/2 \end{pmatrix}, \quad H_1 = \begin{pmatrix} 1/2 & -3/4 \\ 1/8 & -1/8 \end{pmatrix}, \tag{2.11}$$

and  $H_b = 0, \forall b \notin \{-1, 0, 1\}$ .

Another characteristic is the symmetry property. It follows from [11] that the symmetric relation fulfill by these bases as

$$\phi(x) = S\phi(-x), \tag{2.12}$$

where

$$S = \begin{pmatrix} 1 & 0 \\ 0 & -1 \end{pmatrix}.$$

So, the understanding is that  $\phi^1$  and  $\phi^2$  are symmetric and antisymmetric, respectively. It is easy to confirm that

$$H_b = SH_{-b}S, \quad b \in \mathbb{Z}. \tag{2.13}$$

Regarding the construction of biorthogonal wavelets, note that a dual scaling function  $\tilde{\phi} = (\tilde{\phi}^1, \tilde{\phi}^2)$  exists, which generates another MRA  $\tilde{V}_J \subset L_2(\mathbb{R})$ . Due to duality, the biorthogonality condition must be satisfied:

$$\langle \phi, \tilde{\phi}(\cdot - b) \rangle = \delta_{0,b}I_2, \quad b \in \mathbb{Z}, \tag{2.14}$$

where  $\langle \cdot, \cdot \rangle$  denotes the  $L_2$ -inner product and  $I_2$  is  $2 \times 2$  identity matrix.

The multiresolution spaces  $\tilde{V}_J \subset L_2(\mathbb{R})$  are generated by a dual multi-generator  $\tilde{\phi}$ . Biorthogonality implies that the biorthogonality condition must be satisfied by the scaling sequences. In other words, the refinement masks  $\tilde{H}_l, l \in \mathbb{Z}$  are obtained using (2.14) in such a way that they satisfy the following equation

$$\sum_{l \in \mathbb{Z}} H_l \tilde{H}_{l+2b}^T = 2\delta_{0,b}I_2, \quad b \in \mathbb{Z}. \tag{2.15}$$



The refinement masks  $\tilde{H}_l, l \in \mathbb{Z}$  from [11] are:

$$\begin{aligned} \tilde{H}_{-2} &= \begin{pmatrix} -\frac{7}{87} & -\frac{5}{64} \\ \frac{87}{128} & \frac{31}{64} \end{pmatrix}, \quad \tilde{H}_{-1} = \begin{pmatrix} \frac{1}{2} & \frac{3}{16} \\ -\frac{99}{32} & -\frac{37}{32} \end{pmatrix}, \quad \tilde{H}_0 = \begin{pmatrix} \frac{39}{32} & 0 \\ 0 & \frac{15}{8} \end{pmatrix}, \\ \tilde{H}_1 &= \begin{pmatrix} \frac{1}{2} & -\frac{3}{16} \\ \frac{99}{32} & -\frac{37}{32} \end{pmatrix}, \quad \tilde{H}_2 = \begin{pmatrix} -\frac{7}{87} & \frac{5}{64} \\ -\frac{87}{128} & \frac{31}{64} \end{pmatrix}, \end{aligned}$$

with  $\tilde{H}_l = 0$  for  $l \notin -2, \dots, 2$ .

We now define the set  $\varphi = \{\varphi_1, \varphi_2, \dots, \varphi_{2^{J+1}}\}$  whit elements

$$\varphi_{2b+(k-1)} := \phi_{J,b}^k, \quad \text{for } k = 1, 2, \quad b \in \mathcal{J},$$

and  $\varphi_1 := \sqrt{2}\phi_{J,0}^1|_{[0,1]}$ ,  $\varphi_{2^{J+1}} := \sqrt{2}\phi_{J,2^J}^1|_{[0,1]}$ . For any function  $u \in L_2(\mathbb{R})$ , the projection  $\mathcal{P}_J$  maps  $u$  into  $V_J$  as:

$$u(x) \approx \mathcal{P}_J(u)(x) = \sum_{l=1}^{2^{J+1}} c_l \varphi_l(x). \tag{2.16}$$

Using the biorthogonality condition (2.14), the coefficients  $c_l$  are computed by:

$$c_l = \langle u, \tilde{\varphi}_l \rangle = \int_0^1 u(x) \tilde{\varphi}_l(x) dx, \quad \text{for } l = 1, \dots, 2^{J+1}.$$

Alternatively, coefficients can be found without integration using Hermite interpolation:

$$\begin{cases} c_1 := \frac{1}{\sqrt{2}}u(0), \\ c_{2l} = u\left(\frac{l}{2^J}\right), \\ c_{2l+1} = 2^{-J}u'\left(\frac{l}{2^J}\right), \quad l = 1, \dots, 2^J - 1, \\ c_{2^{J+1}} := \frac{1}{\sqrt{2}}u(1). \end{cases} \tag{2.17}$$

Let  $\Phi_J$  be a vector function, whose  $i$ -th element is  $\varphi_i(x)$ . Then (2.16) becomes

$$u(x) \approx C^T \Phi_J(x), \tag{2.18}$$

where  $C$  is the coefficients vector  $\{c_l, l = 1, \dots, 2^{J+1}\}$ .

Following theorem 2 in [9], we can derive a bound for the error of this projection that arises from (2.16).

**Theorem 2.6.** (cf. [9, 27]) *Let  $u : [0, 1] \rightarrow \mathbb{R}$  is the function that belongs to the space of continuous functions with continuous derivatives up to order 4 on  $[0, 1]$  ( $u \in C^4[0, 1]$ ).*

*Then  $\mathcal{P}_J u$  approximates  $u$  with error bound*

$$e_J(x) := |u(x) - \mathcal{P}_J(u)(x)| = \mathcal{C} \mathcal{M}_u \frac{2^{-J}}{1 - 2^{-1}},$$

where

$$\mathcal{M}_u = \max\left\{ \max_{\xi \in [0,1]} |u^{(2)}(\xi)|, \max_{\xi \in [0,1]} |u^{(4)}(\xi)| \right\},$$

and  $\mathcal{C}$  is a constant. Consequently:

$$e_J(x) = O(2^{-J}).$$

Thus,  $e_J(x)$  decays at least as  $2^{-J}$  for sufficiently large  $J$ .



**2.3. Matrix representation of FI operator.** To construct a matrix representation for the FI operator of BHCSSb, as defined in subsection 2.1, we approximate the action of the operator  $\mathcal{I}_0^\kappa$  on the vector function  $\Phi_J(x)$  using the projection  $\mathcal{P}_J$  as follows

$$\mathcal{P}_J(\mathcal{I}_0^\kappa \Phi_J)(x) \approx I_\kappa \Phi_J(x), \tag{2.19}$$

where  $I_\kappa$  is an  $N \times N$  matrix whit  $N = 2^{J+1}$ .

To determine the entries of  $I_\kappa$ , we begin by computing the fractional integral of  $\phi^k(2^J x - b)$ ,  $k = 1, 2$ , viz

$$\mathcal{I}_0^\kappa(\phi^k)(2^J x - b) = \frac{1}{\Gamma(\kappa)} \int_0^x (x - t)^{\kappa-1} \phi^k(2^J t - b) dt, \quad k = 1, 2, \quad b \in \mathcal{J}. \tag{2.20}$$

Due to the support of  $\phi^k(2^J x - b)$ , this integral can be evaluated by considering four cases:

(1) For  $b \in \mathcal{J}$ , if  $x \leq \frac{b-1}{2^J}$ , then

$$\mathcal{I}_0^\kappa(\phi^k)(2^J x - b) = 0.$$

(2) For  $x \in (\frac{b-1}{2^J}, \frac{b}{2^J})$ , the integral (2.20) may be reduced to

$$a_k(x, b) := \mathcal{I}_0^\kappa(\phi^k)(2^J x - b) = \frac{1}{\Gamma(\kappa)} \int_{\frac{b-1}{2^J}}^x (x - t)^{\kappa-1} \phi^k(2^J t - b) dt, \quad \text{for } k = 1, 2.$$

(3) For  $x \in (\frac{b}{2^J}, \frac{b+1}{2^J})$ , let  $b_k(x, b) := \mathcal{I}_0^\kappa(\phi^k)(2^J x - b)$ . Then

$$b_k(x, b) = \frac{1}{\Gamma(\kappa)} \left( \int_{\frac{b-1}{2^J}}^{\frac{b}{2^J}} (x - t)^{\kappa-1} \phi^k(2^J t - b) dt + \int_{\frac{b}{2^J}}^x (x - t)^{\kappa-1} \phi^k(2^J t - b) dt \right),$$

(4) If  $x \geq \frac{b+1}{2^J}$ , then

$$c_k(x, b) := \mathcal{I}_0^\kappa(\phi^k)(2^J x - b) = \frac{1}{\Gamma(\kappa)} \left( \int_{\frac{b-1}{2^J}}^{\frac{b}{2^J}} (x - t)^{\kappa-1} \phi^k(2^J t - b) dt + \int_{\frac{b}{2^J}}^{\frac{b+1}{2^J}} (x - t)^{\kappa-1} \phi^k(2^J t - b) dt \right).$$

The integrals obtained for four cases are calculated explicitly in terms of  $b$ ,  $\kappa$ , and  $J$  for each  $b \in \mathcal{J}$ . Using the Maple command "int(f(t), t = t1..t2)", we compute these integrals analytically. The results can be summarized as

$$T_k(x, b) := \mathcal{I}_0^\kappa(\phi^k)(2^J x - b) = \begin{cases} 0, & x \leq \frac{b-1}{2^J}, \\ a_k(x, b), & \frac{b-1}{2^J} \leq x < \frac{b}{2^J}, \\ b_k(x, b), & \frac{b}{2^J} \leq x < \frac{b+1}{2^J}, \\ c_k(x, b), & x \geq \frac{b+1}{2^J}. \end{cases} \tag{2.21}$$

From Equation (2.7), we express the projection of the fractional integral as:

$$\mathcal{P}_J \mathcal{I}_0^\kappa(\Phi_J)(x) = \mathcal{P}_J(\mathcal{Q}(x)) \approx I_\kappa(\Phi_J)(x), \tag{2.22}$$

where the vector function  $\mathcal{Q}(x)$  is defined by:

$$[\mathcal{Q}(x)]_{2b+(k+1)} = T_k(x, b), \quad b \in \mathcal{J}, \quad k = 1, 2, \tag{2.23}$$

with boundary conditions:

$$\begin{aligned} [\mathcal{Q}(x)]_1 &: T_1(x, 0), \\ [\mathcal{Q}(x)]_{2^{J+1}} &:= T_1(x, 2^J). \end{aligned}$$



Expanding  $Q(x)$  using BHCSSb yields the entries of  $I_\kappa$  (see [9]):

$$I_\kappa = \begin{bmatrix} 0 & A & B_1 & \cdots & \cdots & B_{2^j-2} & Q \\ & Y & H_1 & H_2 & \cdots & H_{2^j-2} & \Theta_1 \\ & & Y & H_1 & \cdots & H_{2^j-3} & \Theta_2 \\ & & & \ddots & \ddots & \vdots & \vdots \\ & & & & Y & H_1 & \vdots \\ & & & & & Y & \Theta_{2^j-1} \\ & & & & & & M \end{bmatrix}, \tag{2.24}$$

where

$$M = \frac{6}{\Gamma(\kappa + 4)} 2^{-J\kappa} (\kappa + 1),$$

$$Q = \frac{1}{\Gamma(\kappa + 4)} \left( (1 - 2^{-J})^\kappa (-12(2^{3J}) + 12\kappa(2^J) + (18 - 6\kappa)2^{2J} - 6\kappa - 6) + 12(2^{3J}) - (18 + 6\kappa) \times 2^{2J} + \kappa^3 + 6\kappa^2 + 11\kappa + 6 \right),$$

and

$$A = \kappa 2^{-J\kappa + \frac{1}{2}} \left[ \frac{\kappa^2 + 6\kappa + 5}{\Gamma(\kappa + 4)} \quad \frac{\kappa^2 + 3\kappa - 4}{\Gamma(\kappa + 3)} \right],$$

$$B_{i-1} = 2^{-J\kappa + \frac{1}{2}} \left[ \eta_{1,1}^{i-1} \quad \eta_{1,2}^{i-1} \right], \quad i = 2, \dots, 2^J - 1,$$

with

$$\eta_{1,1}^{i-1} = -\frac{2^{-J\kappa + \frac{1}{2}}}{\Gamma(\kappa + 4)} \left( i^\kappa (-11\kappa - 6 - 12i^3 + (6\kappa + 18)i^2 - \kappa^3 - 6\kappa^2) + (i - 1)^\kappa (6\kappa + 612i^3 + (6\kappa - 18)i^2 - 12\kappa i) \right),$$

$$\eta_{1,2}^{i-1} = -\frac{2^{-J\kappa + \frac{1}{2}}}{\Gamma(\kappa + 4)} i \left( i^\kappa (12(\kappa + 3)i^3 - 6(6 + \kappa^2 + 5\kappa)i^2 + 11\kappa^2 + 6\kappa^3 + 6\kappa + \kappa^4) + (i - 1)^\kappa (-12(\kappa + 3)i^3 - 6(\kappa^2 + \kappa - 6) + 6(\kappa^2 + 3\kappa)i) \right).$$

The  $2 \times 2$  block matrices are given by

$$Y = 2^{-J\kappa + 1} \begin{bmatrix} \frac{3(\kappa + 1)}{\Gamma(\kappa + 4)} & \frac{3\kappa}{\Gamma(\kappa + 3)} \\ \frac{\kappa}{\Gamma(\kappa + 4)} & \frac{(\kappa - 1)}{\Gamma(\kappa + 3)} \end{bmatrix},$$

$$H_1 = 2^{-J\kappa + 2} \begin{bmatrix} \frac{6(2^\kappa(\kappa - 1) + 1)}{\Gamma(\kappa + 4)} & \frac{3(2^\kappa(\kappa - 2) + 2)}{\Gamma(\kappa + 3)} \\ \frac{2(\kappa + 3 + 2^\kappa(\kappa - 3))}{\Gamma(\kappa + 4)} & \frac{(2^\kappa(\kappa - 4) + 2\kappa + 4)}{\Gamma(\kappa + 3)} \end{bmatrix}.$$



The components of  $H_i = \begin{bmatrix} h_{1,1}^i & h_{1,2}^i \\ h_{2,1}^i & h_{2,2}^i \end{bmatrix}$  for  $i = 1, \dots, 2^J - 2$ , are

$$\begin{aligned} h_{1,1}^i &:= -6 \frac{2^{(-J\kappa)}}{\Gamma(\kappa + 4)} \left( (i - 1)^\kappa (4 - 12i + 2i^2 - 4i^3) + (i - 2)^\kappa (2i^3 + (\kappa - 9)i^2 - 4(\kappa - 3)i + 4\kappa - 4) \right. \\ &\quad \left. + i^{\kappa+2} (2i - (\kappa + 3)) \right), \\ h_{1,2}^i &:= -6 \frac{2^{(-J\kappa)}}{\Gamma(\kappa + 3)} \left( (i - 2)^\kappa (2i^2 + (\kappa - 6)i - 2\kappa + 4) + (i - 1)^\kappa (4i^2 + 8i - 4) + i^\kappa (2i^2 - (\kappa + 2)i) \right), \\ h_{2,1}^i &:= -\frac{2^{(J\kappa+1)}}{\Gamma(\kappa + 4)} \left( i^{\kappa+2} (-3i + \kappa + 3) - 8i(\kappa + 3) + 4\kappa + 12 \right) + (i - 1)^\kappa ((12 + 4\kappa)i^2 \\ &\quad + (i - 2)^\kappa (3i^3 - (15 - \kappa)i^2 - 4(\kappa - 6)i + 4\kappa - 12)), \\ h_{2,2}^i &:= -\frac{2^{(J\kappa+1)}}{\Gamma(\kappa + 3)} \left( (i - 2)^\kappa (3i^2 + (\kappa - 10)i - 2\kappa + 8) - 8 - 4\kappa + (i - 1)^\kappa ((8 + 4\kappa)i) + i^\kappa (-3i^2 + (\kappa + 2)i) \right). \end{aligned}$$

The remaining matrices  $\Theta_i$ , for  $i = 1, \dots, 2^J - 1$  are

$$\Theta_i = \begin{bmatrix} \mu_{1,1}^i & \mu_{1,2}^i \end{bmatrix}^T, \quad i = 1, \dots, 2^J - 1,$$

$$\begin{aligned} \mu_{1,1}^i &:= -\frac{3\sqrt{2}}{\Gamma(\kappa + 4)} \left( \left( \frac{3}{4} - \frac{1}{4}i \right)^\kappa (-2i^3 + (\kappa + 21)i^2 + 9\kappa + 81 - 6(\kappa + 12)i) + \left( 1 - \frac{1}{4}i \right)^\kappa (4i^3 - 48i^2 + 192i - 256) \right. \\ &\quad \left. + \left( \frac{5}{4} - \frac{1}{4}i \right)^\kappa (-2i^3 + (27 - \kappa)i^2 - 10(12 - \kappa)i - 25\kappa + 175) \right), \\ \mu_{1,2}^i &:= -\frac{\sqrt{2}}{\Gamma(\kappa + 4)} \left( \left( \frac{3}{4} - \frac{1}{4}i \right)^\kappa (9\kappa + 108 - (6\kappa + 99)i + (\kappa + 30)i^2 - 3i^3) + \left( 1 - \frac{1}{4}i \right)^\kappa (4(\kappa + 3)i^2 - 32(\kappa + 3)i \right. \\ &\quad \left. + 192 + 64\kappa) + \left( \frac{5}{4} - \frac{1}{4}i \right)^\kappa (3i^3 + (\kappa - 42)i^2 + (-10\kappa + 195)i + 25\kappa - 300) \right). \end{aligned}$$

**Lemma 2.7.** Let  $u \in L_2[0, 1]$  with approximation  $u \approx \mathcal{P}_J(u) := u_J(x) = C^T \Phi_J(x)$ . If  $\mathcal{I}_0^\kappa(u_J)(x)$  is obtained by  $C^T I_\kappa \Phi_J(x)$ , then

$$\lim_{J \rightarrow \infty} \mathcal{I}_0^\kappa(u_J)(x) = \mathcal{I}_0^\kappa(u)(x). \tag{2.25}$$

*Proof.* By Theorem 2.6, the convergence of BHCSSb implies:

$$\lim_{J \rightarrow \infty} u_J(x) := \lim_{J \rightarrow \infty} \mathcal{P}_J(u)(x) = \lim_{J \rightarrow \infty} \sum_{l=1}^{2^{J+1}} c_l \varphi_l(x) = u(x). \tag{2.26}$$

Since the vector function  $\Phi_J(x)$  consists of continuous functions, we have

$$\lim_{J \rightarrow \infty} \int_0^x (x - t)^{\kappa-1} \sum_{l=1}^{2^{J+1}} c_l \varphi_l(t) dt = \lim_{J \rightarrow \infty} \sum_{l=1}^{2^{J+1}} c_l \int_0^x (x - t)^{\kappa-1} \varphi_l(t) dt. \tag{2.27}$$

Consequently, we obtain

$$\lim_{J \rightarrow \infty} \mathcal{I}_0^\kappa(u_J)(x) = \lim_{J \rightarrow \infty} C^T I_\kappa \Phi_J(x). \tag{2.28}$$

Combining Equation (2.28) and Definition 2.1 for  $\kappa \in \mathbb{R}^+$ , yields

$$\Gamma(\kappa) \mathcal{I}_0^\kappa(u)(x) = \int_0^x (x - t)^{\kappa-1} u(t) dt = \lim_{J \rightarrow \infty} \int_0^x (x - t)^{\kappa-1} u_J(t) dt = \Gamma(\kappa) \lim_{J \rightarrow \infty} C^T I_\kappa \Phi_J(x). \tag{2.29}$$



From (2.28) and (2.29), it follows directly that

$$\lim_{J \rightarrow \infty} \mathcal{I}_0^\kappa(u_J)(x) = \mathcal{I}_0^\kappa(u)(x).$$

□

### 3. METHOD DESCRIPTION

This section presents a wavelet Galerkin method algorithm using BHCSSb to solve the FIDE (1.1). The operator form of (1.1) can be expressed as

$$({}^C\mathcal{D}_0^\kappa - c_2\mathcal{K})w = c_1f, \tag{3.1}$$

where the integral operator  $\mathcal{K}$  is defined by

$$\mathcal{K}(w)(x) := \int_{\Omega} k(x, t)g(w(t))dt. \tag{3.2}$$

The uniqueness of the solution to (1.1) follows directly for sufficiently smooth functions  $w(x)$  (see [17]). Since our proposed algorithm reduces the problem to a Volterra-Fredholm integral equation, we establish solution equivalence through the following lemma.

**Lemma 3.1.** (cf [17]) *Assume that  $w, f$ , and  $k$  are continuous functions. The function  $w(x)$  is the solution of (1.1) if and only if it satisfies the VFIE*

$$w(x) = \sum_{i=0}^{\eta-1} \frac{w^{(i)}(0)}{i!} x^i + c_1\mathcal{I}_0^\kappa(f)(x, w(x)) + c_2\mathcal{I}_0^\kappa\mathcal{K}(w)(x), \tag{3.3}$$

where  $\kappa \in \mathbb{R}^+$  and  $\eta = -[-\kappa]$ .

To implement the wavelet Galerkin method, we use the operator  $\mathcal{P}_J$  to expand the unknown solution  $w(x)$  based on BHCSSb, as follows:

$$w(x) \approx \mathcal{P}_J(w)(x) = W^T\Phi_J(x) := w_J(x), \tag{3.4}$$

where  $W$  is a square matrix of order  $N$  with unknown coefficients. Substituting (3.4) into (3.3) we get

$$w_J(x) = \sum_{i=0}^{\eta-1} \frac{w^{(i)}(0)}{i!} x^i + c_1\mathcal{I}_0^\kappa(f)(x, w_J(x)) + c_2\mathcal{I}_0^\kappa\mathcal{K}(w_J)(x). \tag{3.5}$$

In the sequel, all terms into  $V_J$  using the operator  $\mathcal{P}_J$ .

- Let  $u_1(x) := \sum_{i=0}^{\eta-1} \frac{w^{(i)}(0)}{i!} x^i$ . We can obtain

$$u_1(x) \approx \mathcal{P}_J(u_1)(x) = U_1^T\Phi_J(x), \tag{3.6}$$

where the  $l$ -th component of  $U_1$  is calculated by  $\langle u_1, \tilde{\varphi}_l \rangle$ .

- Replacing the approximation  $w_J$  instead of  $w$  into the function  $g(w(t))$  and mapping the obtained function into the space  $V_J$ , we get

$$u_2(t) := g(w_J(t)) \approx \mathcal{P}_J(g(w_J(t))) = G^T\Phi_J(t), \tag{3.7}$$

where the  $l$ -th element of the vector  $G$  is  $\langle u_2, \tilde{\varphi}_l \rangle$ . A similar mapping can be done for the function  $k(x, t)$ , viz

$$k(x, t) \approx \mathcal{P}_J(k)(x, t) = \Phi_J^T(x)K\Phi_J(t), \tag{3.8}$$

in which

$$K_{i,j} = \int_0^1 \int_0^1 k(x, t)\tilde{\varphi}_j(t)\tilde{\varphi}_i(x)dxdt, \quad i, j = 1, 2, \dots, N.$$

Replacing (3.8) into  $\mathcal{K}(w_J)(x)$  and using the operational matrix of product  $Z_{i,j} = \langle \varphi_j, \varphi_i \rangle$ , we obtain

$$\mathcal{P}_J\mathcal{K}(w_J)(x) \approx \Phi_J^T(x)KZ\Phi_J(x) =: p_2(x) \in V_J, \tag{3.9}$$



Note that  $\mathcal{P}_J$  is a bounded projection operator, i.e.,

$$\mathcal{P}_J(w)(x) = w(x), \quad w(x) \in V_J.$$

Equivalently, we obtain  $\mathcal{P}_J^2 = \mathcal{P}_J$ . According to this, the function  $p_2(x)$  can be approximated by using the projection operator  $\mathcal{P}_J$ , and then, we can summarize (3.9) as

$$\mathcal{P}_J \mathcal{K}(w_J)(x) \approx P_2^T \Phi_J(x), \tag{3.10}$$

in which  $P_2$  is a  $N$ -dimensional vector. Using (3.10) and matrix  $I_\kappa$ , the Volterra-Fredholm integral  $\mathcal{I}_0^\kappa \mathcal{K}(w_J)(x)$ , existing in Equation (3.5), can be approximated as

$$\mathcal{I}_0^\kappa \mathcal{K}(w_J)(x) \approx P_2^T I_\kappa \Phi_J(x). \tag{3.11}$$

- Considering the above manner for the previous item, one can approximate  $\mathcal{I}_0^\kappa(f)(x, w(x))$  as follows.

$$\begin{aligned} \mathcal{I}_0^\kappa(f)(x, w_J(x)) &\approx \mathcal{I}_0^\kappa(F^T \Phi_J(x)) \\ &\approx F^T I_\kappa \Phi_J(x), \end{aligned} \tag{3.12}$$

in which the  $l$ -th element of  $N$ -dimensional vector  $F$  is computed by  $\langle f, \tilde{\varphi}_l \rangle$ .

Substituting (3.4), (3.6), (3.11), and (3.12) into (3.5) yields the residual

$$R(x) := (W^T - U_1^T - c_1 F^T I_\kappa - P_2^T I_\kappa) \Phi_J(x) = 0. \tag{3.13}$$

Applying the Galerkin method and the biorthogonality of BHCSSb ( $\langle \Phi_J, \tilde{\Phi}_J \rangle = I_N$ ) yields the system

$$\mathcal{F}(W) = 0, \tag{3.14}$$

where  $\mathcal{F}$  is a nonlinear or linear vector function of  $W$ . The generalized minimal residual method (GMRES method) [32] and Newton’s method are used to determine the unknown vector  $W$  for the linear and nonlinear cases, respectively. It is worth mentioning that Newton’s method is implemented with starting point  $W_0 = O$  (the null vector), and the termination criterion is set to be the absolute residual, i.e.,

$$\|\mathcal{F}(W_n)\| \leq 10^{-16}, n \geq 1.$$

Assuming the linear system (3.14) has the form  $AW = b$ , we implement the GMRES method using the Matlab function "gmres( $A, b, restart, tol$ )", where

- "restart" is the number of inner iterations before restart (this scalar integer is used to control the maximum number of iterations, which in this paper has been chosen equal to 10),
- "tol" is the method tolerance (use this input to control runtime and accuracy in the computing. A smaller value of  $tol$  means the answer should be more precise for the computing to be successful).

In this paper, "tol" is set to  $10^{-16}$ .

### 3.1. Convergence of the method.

**Theorem 3.2.** Consider the continuous functions  $g$  and  $f$  that fulfill the conditions (1.3) and

$$|f(x, w(x)) - f(x, u(x))| \leq \rho |w - u|, \tag{3.15}$$

respectively. Furthermore, we suppose that  $k(x, t)$  is a sufficiently smooth function on  $\Omega \times \mathbb{R}$ .

If  $c_1 \frac{\rho M_1}{\kappa \Gamma(\kappa)} + c_2 \frac{\rho}{\Gamma(\kappa+1)} < 1$  with  $\kappa \in \mathbb{R}^+$ , and  $M_1 := \max_{x,t \in [0,1]} |k(x, t)|$ , then the error of the method satisfies

$$\|w - w_J\|_\infty = O(2^{-J}). \tag{3.16}$$



*Proof.* Considering the Lipschitz condition (1.3) and putting  $M_1 = \max_{x,t \in \Omega} \{k(x,t)\}$ , if the functions  $k$  and  $g$  are continuous, we can verify that

$$\begin{aligned} \|\mathcal{I}_0^\kappa \mathcal{K}(w) - \mathcal{I}_0^\kappa \mathcal{K}(w_J)\| &= \|\mathcal{I}_0^\kappa \left( \int_\Omega k(x,t)g(w(t))dt - \int_\Omega k(x,t)g(w_J(t))dt \right)\| \\ &\leq \|\mathcal{I}_0^\kappa \left( \rho \int_\Omega k(x,t)(w(t) - w_J(t))dt \right)\| \\ &\leq \|\mathcal{I}_0^\kappa \left( \rho M_1 \int_\Omega (w(t) - w_J(t))dt \right)\| \\ &\leq \frac{M_1 \rho}{\Gamma(\kappa)} \int_0^x (x-t)^{\kappa-1} \int_\Omega \|w - w_J\| dx dt \\ &\leq \frac{M_1 \rho}{\Gamma(\kappa)} \|w - w_J\| \int_0^x (x-t)^{\kappa-1} dt \\ &\leq \frac{M_1 \rho}{\kappa \Gamma(\kappa)} \|w - w_J\|. \end{aligned} \tag{3.17}$$

Using Theorem 2.6, we have

$$\|\mathcal{I}_0^\kappa \mathcal{K}(w_J) - \mathcal{P}_J \mathcal{I}_0^\kappa \mathcal{K}(w_J)\| \leq C_2 M_2 2^{-J}, \tag{3.18}$$

where  $M_2 := \max\{\max_{\xi \in \Omega} |\mathcal{D}^2 \mathcal{I}_0^\kappa \mathcal{K}(w_J)(\xi)|, \max_{\xi \in \Omega} |\mathcal{D}^4 \mathcal{I}_0^\kappa \mathcal{K}(w_J)(\xi)|\}$ . To approximate  $M_2$ , there are two situations:

(1) if  $n < \eta$ , then we have

$$\mathcal{D}^n \mathcal{I}_0^\kappa \mathcal{K}(w_J) = \mathcal{I}_0^{\kappa-n} \mathcal{K}(w_J), \tag{3.19}$$

and it follows from Lemma 2.2 that

$$\begin{aligned} \|\mathcal{D}^n \mathcal{I}_0^\kappa \mathcal{K}(w_J)\| &= \|\mathcal{I}_0^{\kappa-n} \mathcal{K}(w_J)\| \leq \frac{1}{\Gamma(\kappa - n + 1)} \|\mathcal{K}(w_J)\| \\ &\leq \frac{M_1}{\Gamma(\kappa - n + 1)} \left\| \int_\Omega g(w_J(t)) dt \right\| \\ &\leq \frac{M_1}{\Gamma(\kappa - n + 1)} \int_\Omega \|g(w_J(t))\| dt, \end{aligned} \tag{3.20}$$

Consequently, the norm  $\|\mathcal{D}^n \mathcal{I}_0^\kappa \mathcal{K} w_J\|$  is bounded by the continuity of the function  $g$ .

(2) Let  $n \geq \eta$ . We refer to Lemma 2.21 [17] to show that

$$\mathcal{D}^n \mathcal{I}_0^\kappa \mathcal{K}(w_J) = {}^C \mathcal{D}^{n-\kappa} \mathcal{D}^\kappa \mathcal{I}_0^\kappa \mathcal{K}(w_J) = {}^C \mathcal{D}^{n-\kappa} \mathcal{K}(w_J). \tag{3.21}$$

Using Lemma 2.5, after taking the norm from both sides of (3.21), we can write

$$\begin{aligned} \|\mathcal{D}^n \mathcal{I}_0^\kappa \mathcal{K}(w_J)\| &= \|\mathcal{D}^{n-\kappa} \mathcal{K}(w_J)\| \\ &\leq \frac{1}{\Gamma(m - n + \kappa)(m - n + \kappa + 1)} \|\mathcal{K}(w_J)\|, \quad (m = [n - \kappa] + 1). \end{aligned} \tag{3.22}$$

Thus, for both cases, we prove that the norm  $\|\mathcal{D}^n \mathcal{I}_0^\kappa \mathcal{K} w_J\|$  is bounded.

According to the hypothesis, because  $f(x, u(x))$  fulfills the Lipschitz condition (1.3), the norm of  $(\mathcal{I}_0^\kappa(f)(x, w(x)) - \mathcal{I}_0^\kappa(f)(x, w_J(x)))$  can be bounded using Lemma 2.2, as follows:

$$\begin{aligned} \|\mathcal{I}_0^\kappa(f)(x, w(x)) - \mathcal{I}_0^\kappa(f)(x, w_J(x))\| &\leq \varrho \|\mathcal{I}_0^\kappa(w - w_J)\| \\ &\leq \frac{\varrho}{\Gamma(\kappa + 1)} \|w - w_J\|. \end{aligned} \tag{3.23}$$

Using Theorem 2.6, we can write

$$\|\mathcal{I}_0^\kappa(f)(x, w_J) - \mathcal{P}_J \mathcal{I}_0^\kappa(f)(x, w_J)\| \leq C_3 M_3 2^{-J}, \tag{3.24}$$



where

$$M_3 := \max\left\{ \max_{\xi \in [0,1]} |\mathcal{D}^2 \mathcal{I}_0^\kappa f(\xi, w_J(\xi))|, \max_{\xi \in [0,1]} |\mathcal{D}^4 \mathcal{I}_0^\kappa f(\xi, w_J(\xi))| \right\}.$$

To evaluate the approximate value of  $M_3$ , we follow the two cases that were investigated for  $M_2$ . However, we omit the evaluation due to its simplicity and similarity to  $M_2$ .

Subtracting (3.3) from

$$w_J(x) = \mathcal{P}_J(p_1)(x) + c_1 \mathcal{P}_J(\mathcal{I}_0^\kappa(f))(x, w_J(x)) + c_2 \mathcal{P}_J(\mathcal{I}_0^\kappa(\mathcal{K}))(w_J)(x), \tag{3.25}$$

we obtain

$$\begin{aligned} w(x) - w_J(x) &= p_1 - \mathcal{P}_J(p_1) + c_1 \mathcal{I}_0^\kappa(f)(x, w(x)) - c_1 \mathcal{P}_J \mathcal{I}_0^\kappa(f)(x, w_J(x)) + c_2 \mathcal{I}_0^\kappa \mathcal{K}(w)(x) \\ &\quad - c_2 \mathcal{P}_J \mathcal{I}_0^\kappa \mathcal{K}(w_J)(x) + c_1 \mathcal{I}_0^\kappa(f)(x, w_J(x)) - c_1 \mathcal{I}_0^\kappa(f)(x, w_J(x)) \\ &\quad + c_2 \mathcal{I}_0^\kappa \mathcal{K}(w_J)(x) - c_2 \mathcal{I}_0^\kappa \mathcal{K}(w_J)(x), \end{aligned} \tag{3.26}$$

where  $u_1(x) := \sum_{i=0}^{n-1} \frac{w^{(i)}(0)}{i!} x^i$ . After taking the norm from both sides of (3.26), we employ Equations (3.17), (3.18), (3.23), (3.24), and apply the triangle inequality to indicate that

$$\begin{aligned} \|w - w_J\| &\leq \|u_1 - \mathcal{P}_J(u_1)\| + c_1 \|\mathcal{I}_0^\kappa(f)(x, w(x)) - \mathcal{I}_0^\kappa(f)(x, w_J(x))\| \\ &\quad + c_1 \|\mathcal{I}_0^\kappa(f)(x, w_J(x)) - c_1 \mathcal{P}_J \mathcal{I}_0^\kappa(f)(x, w_J(x))\| \\ &\quad + c_2 \|\mathcal{I}_0^\kappa \mathcal{K}(w)(x) - \mathcal{I}_0^\kappa \mathcal{K}(w_J)(x)\| \\ &\quad + c_2 \|\mathcal{I}_0^\kappa \mathcal{K}(w_J)(x) - \mathcal{P}_J(\mathcal{I}_0^\kappa \mathcal{K}(w_J)(x))\| \\ &\leq C_4 M_4 2^{-J} + c_1 \frac{\rho M_1}{\kappa \Gamma(\kappa)} \|w - w_J\| + c_1 C_2 M_2 2^{-J} \\ &\quad + c_2 \frac{\varrho}{\Gamma(\kappa + 1)} \|w - w_J\| + c_2 C_3 M_3 2^{-J} \\ &= \left( c_1 \frac{\rho M_1}{\kappa \Gamma(\kappa)} + c_2 \frac{\varrho}{\Gamma(\kappa + 1)} \right) \|w - w_J\| + (C_4 M_4 + c_1 C_2 M_2 + c_2 C_3 M_3) 2^{-J}, \end{aligned} \tag{3.27}$$

where  $\|u_1 - \mathcal{P}_J(u_1)\| \leq C_4 M_4 2^{-J}$  with

$$M_4 := \max\left\{ \max_{\xi \in [0,1]} |\mathcal{D}^2 u_1(\xi)|, \max_{\xi \in [0,1]} |\mathcal{D}^4 u_1(\xi)| \right\}.$$

By setting  $\lambda := c_1 \frac{\rho M_1}{\kappa \Gamma(\kappa)} + c_2 \frac{\varrho}{\Gamma(\kappa+1)}$ , if  $\lambda < 1$ , then we obtain

$$\|w(x) - w_J(x)\| \leq \frac{C}{1 - \lambda} 2^{-J}, \tag{3.28}$$

where  $C := C_4 M_4 + c_1 C_2 M_2 + c_2 C_3 M_3$ . □

#### 4. NUMERICAL EXPERIMENTS

To demonstrate the accuracy and efficiency of the presented algorithm, some illustrative examples are provided in this section. To this end, we introduce several error criteria as follows:

- The  $L_\infty$ -error is obtained by

$$\|w(x) - w_J(x)\|_\infty = \sup\{|w(x) - w_J(x)| : x \in [0, 1]\}.$$

- The  $L_2$ -error is calculated by

$$\|w(x) - w_J(x)\|_2 = \left( \int_0^1 |w(x) - w_J(x)|^2 dx \right)^{1/2}.$$



TABLE 1. The  $L_2$ -error for increasing values of the parameter  $J$ , compared with Alpert’s multi-wavelets method for Example 4.1.

	Presented method			[28]
	$J = 3$	$J = 4$	$J = 5$	$r = 3, J = 5$
$L_2$ -error	$3.5325 \times 10^{-3}$	$1.5752 \times 10^{-3}$	$7.0524 \times 10^{-4}$	$1.4297 \times 10^{-3}$
	$J = 6$	$J = 7$	$J = 8$	
$L_2$ -error	$3.2012 \times 10^{-4}$	$1.4912 \times 10^{-4}$	$6.9567 \times 10^{-5}$	

TABLE 2. The  $L_\infty$ -error for Example 4.1.

$x$	0.1	0.3	0.5	0.7	0.9
J=3	$2.74 \times 10^{-3}$	$4.30 \times 10^{-3}$	$3.13 \times 10^{-3}$	$2.66 \times 10^{-3}$	$2.05 \times 10^{-3}$
J=4	$2.07 \times 10^{-3}$	$1.67 \times 10^{-3}$	$1.43 \times 10^{-3}$	$1.19 \times 10^{-3}$	$9.04 \times 10^{-3}$
J=5	$1.02 \times 10^{-3}$	$7.90 \times 10^{-4}$	$7.62 \times 10^{-4}$	$5.70 \times 10^{-4}$	$4.50 \times 10^{-4}$
$x$	0.91	0.93	0.95	0.97	0.99
J=3	$2.02 \times 10^{-3}$	$1.96 \times 10^{-3}$	$1.89 \times 10^{-3}$	$1.83 \times 10^{-3}$	$1.76 \times 10^{-3}$
J=4	$8.96 \times 10^{-4}$	$8.77 \times 10^{-4}$	$8.41 \times 10^{-4}$	$8.11 \times 10^{-4}$	$7.84 \times 10^{-4}$
J=5	$4.11 \times 10^{-4}$	$3.77 \times 10^{-4}$	$3.90 \times 10^{-4}$	$3.36 \times 10^{-4}$	$3.77 \times 10^{-4}$

- Root Mean Square Error (RMSE) is used to demonstrate the standard deviation of the residuals and is determined as

$$RMSE = \left( \frac{1}{N} \sum_{i=1}^N |w(x_i) - w_J(x_i)|^2 \right)^{1/2},$$

in which  $N$  is sample size and  $x_i := i/N$ .

According to our analysis, the rate of convergence is  $O(2^{-J})$ . Thus, we expect that when the refinement parameter increases from  $J$  to  $J + 1$ , the error is approximately halved, and the rate of convergence is approximately 1, i.e.,

$$\log_2 \frac{u - u_{J+1}}{u - u_J} \approx \log_2 \frac{2^{J+1}}{2^J} = 1.$$

To verify our analysis, in all following examples, we will demonstrate that increasing the refinement parameter from  $J$  to  $J + 1$  results in the error being approximately halved, with a convergence rate of approximately 1.

**Example 4.1.** Consider the FIDEs from [28]

$${}^C \mathcal{D}_0^{5/6} w(x) + \int_0^1 x e^t (w(t))^2 dt = \frac{3}{\Gamma(1/6)} \left( 2\sqrt[6]{x} - \frac{432}{91} \sqrt[6]{x^{13}} \right) + x(674 - 248e),$$

with the initial condition  $w(0) = 0$ . The exact solution, as given in [28], is  $w(x) = x - x^3$ .

Table 1 shows how the error decreases as parameter  $J$  increases. For the same value of  $J$ , our algorithm yields more accurate results than Alpert’s multiwavelets method. Table 2 presents the  $L_\infty$ -error for different values for  $x$  and  $J$ . Figure 1 displays the approximate solution and  $L_\infty$ -error for  $J = 5$ .

**Example 4.2.** Consider the nonlinear FIDEs from [28]

$${}^C \mathcal{D}_0^{1/2} w(x) + \int_0^1 x t (w(t))^4 dt = \frac{1}{\Gamma(1/2)} \left( 8/3 x^{3/2} - 2x^{1/2} \right) - \frac{x}{1260}, \quad x \in [0, 1],$$

with initial condition  $w(0) = 0$ . The exact solution, as reported in [28], is  $u(x) = x^2 - x$ .



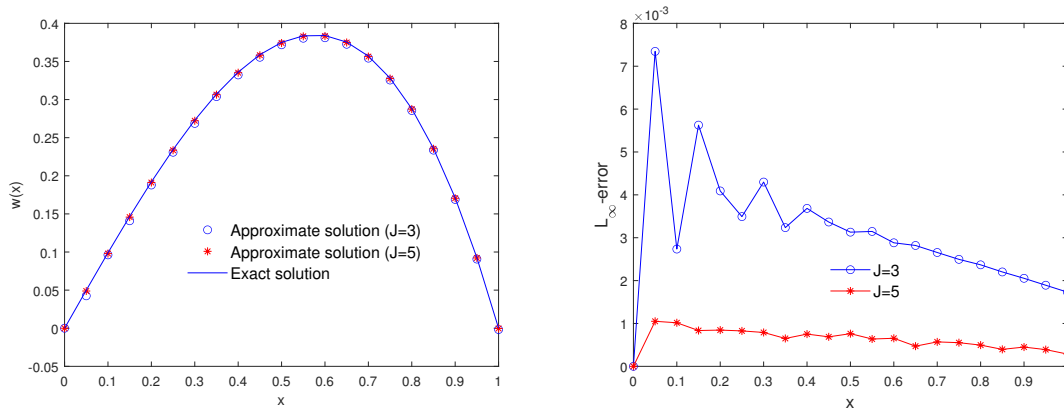


FIGURE 1. Plots of the estimated solution and corresponding  $L_\infty$ -error for Example 4.1.

TABLE 3. The obtained  $L_2$ -error due to the increase of the parameter  $J$  and compare the results with Alpert’s multiwavelets method for Example 4.2.

	Proposed method			Alpert’s multiwavelets method [28]
	$J = 2$	$J = 3$	$J = 4$	$r = 3, J = 5$
$L_2$ -error	$1.8185 \times 10^{-3}$	$6.7717 \times 10^{-4}$	$2.5194 \times 10^{-4}$	$4.1661 \times 10^{-4}$
	$J = 5$	$J = 6$	$J = 7$	
$L_2$ -error	$1.0069 \times 10^{-4}$	$4.0435 \times 10^{-5}$	$1.7794 \times 10^{-5}$	

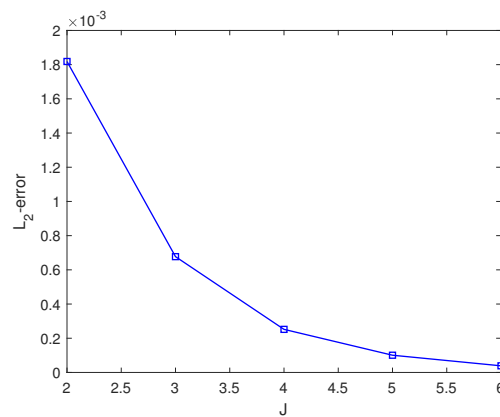


FIGURE 2. The reduction in  $L_2$ -error corresponding to the increase of  $J$  for Example 4.2.

In Table 3, the efficacy of parameter  $J$  and its effect on  $L_2$ -error are illustrated, and a comparison between the presented method and Alpert’s multiwavelets method is reported. For more illustration, Figure 2 is plotted to indicate the effect of  $J$ . Figure 3 demonstrates the approximate solution when the parameter  $J$  is changed and provides a good view of accuracy. Due to the good accuracy of the presented method, the plots of the solutions are very close to each other and close to the exact solution.



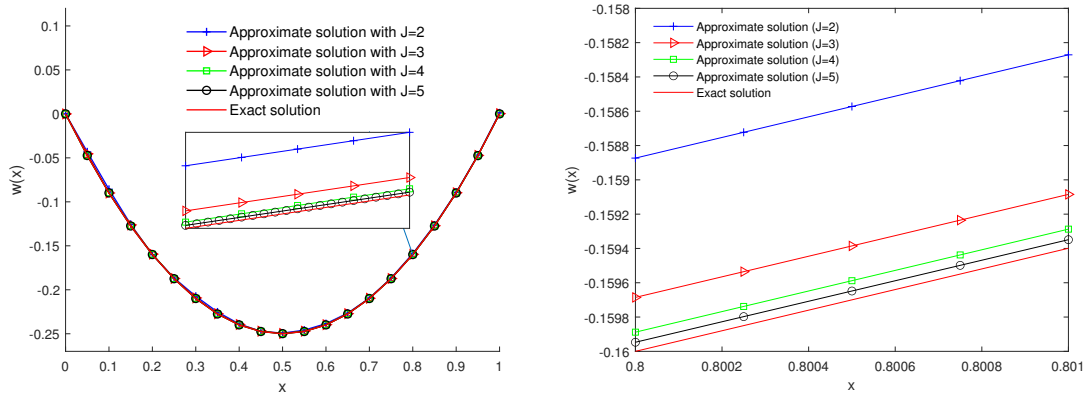


FIGURE 3. Plots of the approximate solution and a zoom of inner sub-figure of Example 4.2, taking different values for  $J$ .

TABLE 4. The obtained  $L_2$ -error and RMSE for different values of  $J$  in Example 4.3.

$J$	2	3	4	5	6
RMSE	$1.3133 \times 10^{-2}$	$7.3342 \times 10^{-3}$	$4.0678 \times 10^{-3}$	$2.2394 \times 10^{-3}$	$1.3234 \times 10^{-3}$
$L_2$ -error	$2.0705 \times 10^{-2}$	$1.1056 \times 10^{-2}$	$5.8400 \times 10^{-3}$	$3.0775 \times 10^{-3}$	$1.6153 \times 10^{-3}$
order	—	0.90512	0.92083	0.92418	0.93002

**Example 4.3.** In this example, we focus on the nonlinear FIDEs

$${}^C \mathcal{D}_0^\kappa u(x) + 3x^2 u^4(x) - \int_0^1 x^2(t+1)w^2(t)dt = \frac{18x^4\Gamma(\frac{3}{2} - \kappa) - 5x^2\Gamma(\frac{3}{2} - \kappa) + 3\sqrt{\pi}x^{1/2-\kappa}}{6\Gamma(\frac{3}{2} - \kappa)},$$

where  $0 < \kappa \leq 1$ . The exact solution is  $w(x) = \sqrt{x}$ .

Table 4 shows how the  $L_2$ -error, RMSE, and the order of convergence change with different values of  $J$ . It is important to note that in practical applications, when the exact solution lacks continuous derivative near the origin, standard numerical methods often fail to achieve accurate solutions. However, by increasing the refinement level  $J$  when using BHCSSb, we can overcome this issue thanks to the multi-scale property of wavelet systems.

Figure 4 demonstrates the effect of the refinement level  $J$  on the solution accuracy. As shown in Figures 4 and 5, the numerical solution converges to the exact one, even in the vicinity of the origin.

**Example 4.4.** We devote the fourth example to the linear equation

$${}^C \mathcal{D}_0^\kappa w(x) - \int_0^1 xtw(t)dt = 3x^2 - \frac{x}{5},$$

with  $w(0) = 0$ . The exact solution for this equation in the case of  $\kappa = 1$  is  $w(x) = x^3$ . Figure 6 the numerical solution for  $J = 4$  and various  $0 < \kappa \leq 1$ . Note that as  $\kappa \rightarrow 1$ , the numerical solution approaches  $w(x) = x^3$ . Table 5 presents the  $L_2$ -error, RMSE, and condition number of the coefficient matrix (3.14) for  $\kappa = 1$ .

**Example 4.5.** As our final example, consider the linear FIDE

$${}^C \mathcal{D}_0^{0.5} w(x) - \int_\Omega (x+t)w(t)dt = f(x),$$



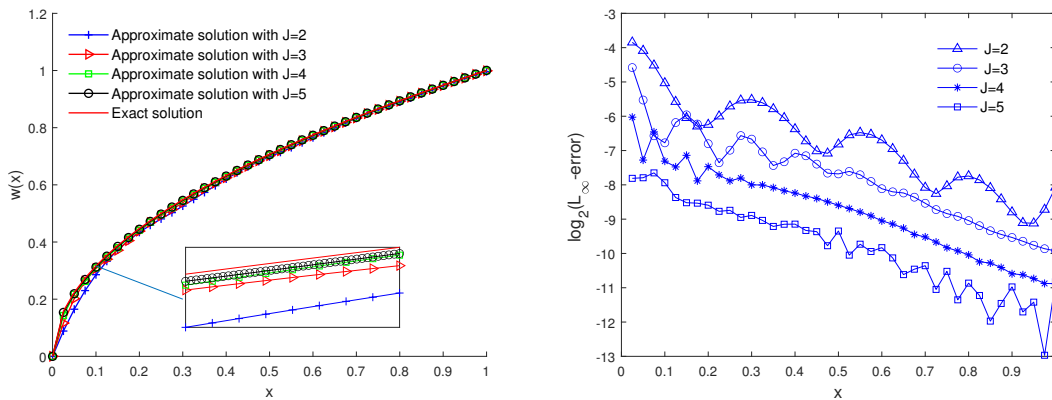


FIGURE 4. Numerical solution and corresponding  $L_\infty$ -error for Example 4.3.

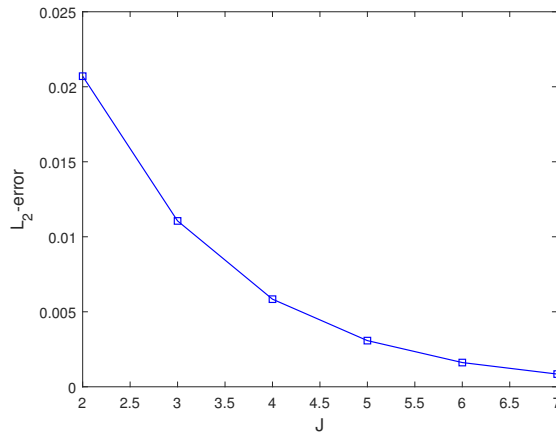


FIGURE 5. Reduction in  $L_2$ -error with increasing  $J$  for Example 4.3.

TABLE 5. Effect of parameter  $J$  on  $L_2$ -error, RMSE, and condition number  $\kappa = 1$  for Example 4.4.

$J$	3	4	5	6	7
RMSE	$2.2821 \times 10^{-6}$	$1.1803 \times 10^{-6}$	$6.0204 \times 10^{-7}$	$3.1747 \times 10^{-7}$	$1.6081 \times 10^{-7}$
$L_2$ -error	$1.6147 \times 10^{-6}$	$8.3508 \times 10^{-7}$	$4.2596 \times 10^{-7}$	$2.2461 \times 10^{-7}$	$1.1378 \times 10^{-7}$
order	—	0.95125	0.97120	0.97325	0.98125
Condition number	1.55019	1.57914	2.01282	2.06217	2.15241

with  $w(0) = 0$  and

$$f(x) = \sqrt{2}S\left(\frac{\sqrt{2x}}{\sqrt{\pi}}\right) \sin(x) + \sqrt{2}C\left(\frac{\sqrt{2x}}{\sqrt{\pi}}\right) \cos(x) + \cos(1)x - \sin(1) + \cos(1) - x,$$



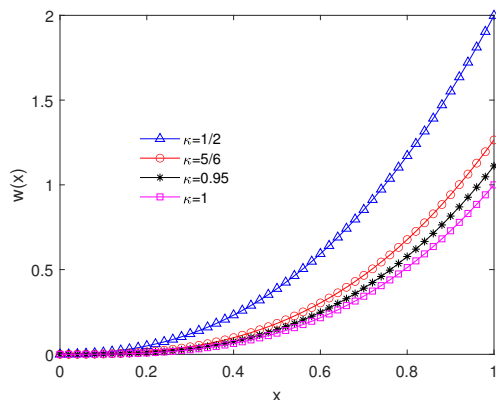


FIGURE 6. Numerical solution of Example 4.4 for  $J = 4$  and various  $\kappa$  values.

TABLE 6. Effect of the parameter  $J$  on  $L_2$ -error, RMSE, and condition number for Example 4.5.

$J$	3	4	5	6	7
RMSE	$1.9756 \times 10^{-3}$	$7.0627 \times 10^{-4}$	$2.7144 \times 10^{-4}$	$1.2876 \times 10^{-4}$	$3.0192 \times 10^{-5}$
$L_2$ -error	$1.9405 \times 10^{-3}$	$7.0444 \times 10^{-4}$	$2.8009 \times 10^{-4}$	$1.4215 \times 10^{-4}$	$6.0484 \times 10^{-5}$
order	—	1.461867	1.330585	1.215453	1.090101
Condition number	15.042517	15.190189	15.728786	15.952871	16.152359

where the Fresnel integrals  $\mathcal{S}(x)$  and  $\mathcal{C}(x)$  are defined as

$$\mathcal{C}(x) = \sum_{i=0}^{\infty} (-1)^i \frac{x^{4i+3}}{(2i+1)!(4i+3)},$$

and

$$\mathcal{S}(x) = \sum_{i=0}^{\infty} (-1)^i \frac{x^{4i+1}}{(2i)!(4i+1)}.$$

The exact solution is  $w(x) = \sin(x)$ .

Table 6 is reported to display the effect of parameter  $J$  on the  $L_2$ -error, RMSE, order of convergence, and condition number. Tables 5 and 6 confirm our convergence analysis from the previous section.

### 5. CONCLUSION

In this work, we have developed a numerical method for solving FIDEs by first reducing them to a Volterra-Fredholm integral equation (VFIE) with weakly singular kernel. The wavelet Galerkin method is then applied to estimate the numerical behavior of the VFIE. To this end, a matrix representation of the fractional integral based on BHCSSb is presented, and we use it to reduce the problem to a system of algebraic equations. The combination of singularity and the challenge related to nonlinearity poses a formidable obstacle in solving the desired equations, but our method overcomes them well. Method convergence is proved, and our investigation verifies that the convergence rate is  $O(2^{-J})$  where  $J \in \mathbb{Z}^+ \cup \{0\}$  is the refinement level. The numerical examples confirm our theoretical analysis. The results illustratively show the efficiency and accuracy of the method, and a comparison between the present method and others demonstrates the accuracy and effectiveness of the method.



## REFERENCES

- [1] B. Alpert, G. Beylkin, R. R. Coifman, and V. Rokhlin, *Wavelet-like bases for the fast solution of second-kind integral equations*, SIAM J. Sci. Statist. Comput., *14*(1) (1993), 159–184.
- [2] H. Aminikhah, *A new analytical method for solving systems of linear integro-differential equations*, J. King Saud Univer. Sci., *23*(4) (2011), 349–353.
- [3] C. N. Angstmann, B. I. Henry, and A. V. McGann, *A fractional order recovery SIR model from a stochastic process*, Bull. Math. Biol., *78*(3) (2016), 468–499.
- [4] A. Arikoglu and I. Ozkol, *Solution of fractional integro-differential equations by using fractional differential transform method*, Chaos, Solitons & Fractals, *40* (2009), 521–529.
- [5] M. Asadzadeh and B. N. Saray, *On a multiwavelet spectral element method for integral equation of a generalized Cauchy problem*, BIT Numerical Mathematics, *62* (2022), 383–1416.
- [6] M. S. Asl, M. Javidi, and Y. Yan, *A novel high-order algorithm for the numerical estimation of fractional differential equations*, J. Comput. Appl. Math., *342* (2018), 180–201.
- [7] R. L. Bagley and P. J. Torvik, *Fractional Calculus in the Transient Analysis of Viscoelastically Damped Structures*, AIAA. J., *23*(6) (1985), 918–925.
- [8] R. T. Baillie, *Long Memory Processes and Fractional Integration in Econometrics*, J. Econometrics, *73*(1) (1996), 5–59.
- [9] H. Bin Jebreen and I. Dassios, *A Biorthogonal Hermite Cubic Spline Galerkin Method for Solving Fractional Riccati Equation*, Mathematics, *10*(9) (2022), 1461.
- [10] V. Daftardar-Gejji, Y. Sukale, and S. Bhalekar, *A new predictorcorrector method for fractional differential equations*, Appl. Math. Comput., *244* (2014), 158–182.
- [11] W. Dahmen, B. Han, R.Q. Jia, and A. Kunoth, *Biorthogonal multiwavelets on the interval: Cubic Hermite splines*, Constr. Approx., *16* (2000), 221–259.
- [12] K. Diethelm, *The analysis of fractional differential equations, An Application-Oriented Exposition Using Differential Operators of Caputo Type*, Springer-Verlag Berlin Heidelberg, 2010.
- [13] K. Diethelm, N. Ford, and A. Freed, *Detailed error analysis for a fractional Adams method*, Numer. Algorithms, *36*(1) (2004), 31–52.
- [14] M. R. Eslahchi, M. Dehghan, and M. Parvizi, *Application of the collocation method for solving nonlinear fractional integro-differential equations*, J. Comput. Appl. Math., *257* (2014), 105–128.
- [15] J. H. He, *Nonlinear Oscillation with Fractional Derivative and its Applications*, International Conference on Vibrating Engineering, (1998), 288–291.
- [16] J. H. He, *Some Applications of Nonlinear Fractional Differential Equations and Their Approximations*, Bull. Sci. Technol., *2* (1999), 86–90.
- [17] A. Kilbas, H. M. Srivastava, and J. J. Trujillo, *Theory and applications of fractional differential equations*, 24. Elsevier B. V., Amsterdam, 2006.
- [18] X. Li, *Numerical solution of fractional differential equations using cubic B-spline wavelet collocation method*, Commun. Nonlinear Sci. Numer. Simulat., *17*(10) (2012), 3934–3946.
- [19] F. Mainardi, *Fractional Calculus: Some Basic Problems in Continuum and Statistical Mechanics. Fractals and Fractional Calculus in Continuum Mechanics*, New York, Springer Verlag, 1997.
- [20] B. Mandelbrot, *Some Noises with  $1/f$  Spectrum, a Bridge between direct Current and White Noise*, IEEE Trans Inform Theory, *2* (1967), 289–298.
- [21] M. Meerschaert and C. Tadjeran, *Finite Difference Approximations for Two-Sided Space-Fractional Partial Differential Equations*, Appl. Numer. Math., *56*(1) (2006), 80–90.
- [22] E. M. Mendes, G. H. Salgado, and L. A. Aguirre, *Numerical solution of caputo fractional differential equations with infinity memory effect at initial condition*, Commun. Nonlinear Sci. Numer. Simulat., *69* (2019), 237–247.
- [23] R. Metzler and J. Klafter, *The Restaurant at the End of the Random Walk: Recent Developments in the Description of Anomalous Transport by Fractional Dynamics*, Journal of Physics A: Mathematical and General, *37* (2004), 161–208.



- [24] S. Momani and K. Al-Khaled, *Numerical Solutions for Systems of Fractional Differential Equations by the Decomposition Method*, Appl. Math. Comput., 162(3) (2005), 1351–1365.
- [25] S. Momani and M. A. Noor, *Numerical methods for fourth order fractional integro-differential equations*, Appl. Math. Comput., 182 (2006), 754–760.
- [26] S. Momani and A. Qaralleh, *An Efficient Method for Solving Systems of Fractional Integro-Differential Equations*, Comput. Math. Appl., 52 (2006), 459–470.
- [27] E. Pourfattah, M. Jahangiri Rad, and B. Nemati Saray, *An efficient algorithm based on the Pseudospectral method for solving Abel's integral equation using Hermite cubic spline scaling bases*, Appl. Numer. Math., 185 (2023), 434–445.
- [28] S. Paseban-Hag, E. Osgooei, and E. Ashpazzadeh, *Alpert wavelet system for solving fractional nonlinear Fredholm integro-differential equations*, Comput. Methods Differ. Equ., 9(3) (2021), 762–773.
- [29] P. Rahimkhani, Y. Ordokhani, and E. Babolian, *A New Operational Matrix based on Bernoulli Wavelets for Solving Fractional Delay Differential Equations*, Numer. Algorithms., 74 (2017), 223–245.
- [30] E. A. Rawashdeh, *Numerical solution of fractional integro-differential equations by collocation method*, Appl. Math. Comput., 176 (2006), 1–6.
- [31] Y. A. Rossikhin and M. V. Shitikova, *Applications of Fractional Calculus to Dynamic Problems of Linear and Nonlinear Hereditary Mechanics of Solids*, Appl. Mech. Rev., 50(1) (1997), 15–67.
- [32] Y. Saad and M. H. Schultz, *GMRES: A generalized minimal residual method for solving nonsymmetric linear systems*, SIAM J. Sci. Stat. Comput., 7 (1986), 856–869.
- [33] H. Saeedi, M. Mohseni Moghadam, N. Mollahasani, and G. N. Chuev, *A CAS wavelet method for solving nonlinear Fredholm integro-differential equations of fractional order*, Commun. Nonl. Sci. Numer. Simul., 16 (2011), 1154–1163.
- [34] P. K. Sahu and S. S. Ray, *A numerical approach for solving nonlinear fractional Volterra-Fredholm integro-differential equations with mixed boundary conditions*, Int. J. Wavelets Multi., 14(5) (2016), 1650036.
- [35] G. H. O. Salgado and L. A. Aguirre, *A hybrid algorithm for Caputo fractional differential equations*, Commun. Nonlinear Sci. Numer. Simulat., 33 (2016), 133–140.
- [36] B. N. Saray, *Abel's integral operator: sparse representation based on multiwavelets*, BIT Numerical Mathematics, 61 (2021), 587–606.
- [37] B. N. Saray, *An efficient algorithm for solving Volterra integro-differential equations based on Alpert's multi-wavelets Galerkin method*, J. Comput. Appl. Math., 348 (2019), 453–465.
- [38] Y. Yan, K. Pal, and N. Ford, *Higher order numerical methods for solving fractional differential equations*, BIT Numerical Mathematics, 54 (2014) 555–584.
- [39] L. Zhu and Q. Fan, *Solving fractional nonlinear Fredholm integro-differential equations by the second kind Chebyshev wavelet*, Commun. Nonlinear Sci. Numer. Simulat., 17 (2012), 2333–2341.

